Scilight

Smart Materials and Devices

https://www.sciltp.com/journals/smd

Review

Advanced Applications for Smart-Metallic Materials

Rongzhi Li [1], Peter K. Liaw [2], Jianzhong Jiang [3] and Yong Zhang [1,3,*]

[1] Beijing Advanced Innovation Center of Materials Genome Engineering, State Key Laboratory for Advanced Metals and Materials, University of Science and Technology Beijing, Beijing 100083, China
[2] Department of Materials Science and Engineering, The University of Tennessee, Knoxville, TN 37996, USA
[3] School of Materials Science and Engineering, Fuyao University of Science and Technology, Fuzhou 350109, China
* Correspondence: drzhangy@ustb.edu.cn; Tel.: +86-186-0008-0235

How To Cite: Li, R.; Liaw, P.K.; Jiang, J.; et al. Advanced Applications for Smart-Metallic Materials. *Smart Materials and Devices* **2025**, *1*(1), 1.

Received: 7 April 2025
Revised: 6 May 2025
Accepted: 15 May 2025
Published: 23 May 2025

Abstract: Smart metallic materials, recognized for their responsiveness to external stimuli, have garnered significant attention in advanced technological applications. This review focuses on three pivotal smart materials: high-entropy alloys (HEAs), shape-memory alloys (SMAs), and soft magnetic materials, addressing their processing techniques, properties, and applications. HEAs, characterized by their multi-principal elemental compositions, exhibit exceptional mechanical strength, corrosion resistance, and thermal stability, positioning them as promising candidates for extreme environments. SMAs, renowned for their ability to recover original shapes under thermal or mechanical stimuli, find widespread use in actuators, sensors, and biomedical devices. Soft magnetic materials, with low hysteresis loss and high permeability, are critical for energy-efficient systems, such as electric motors and transformers. The review further explores diverse processing methodologies, including conventional melting, Taylor wire fabrication, and advanced additive manufacturing (e.g., 3D printing), which enable precise control over microstructures, material properties, and component design to enhance performance and functionality. Emphasis is placed on the integration of these materials into smart systems, highlighting their synergistic roles in emerging technologies. Challenges, such as material stability, scalability of processing techniques, and the development of multifunctional composites, are critically discussed. Finally, future research directions are outlined to address these limitations and advance the field toward next-generation intelligent material systems. This comprehensive analysis aims to bridge the gap between material design, processing innovation, and practical applications, offering insights for researchers and engineers in optimizing smart material solutions.

Keywords: smart metallic materials; high-entropy alloys; shape-memory alloys; soft magnetic materials; additive manufacturing; multifunctional integration

1. Introduction

Intelligent materials represent a class of substances endowed with exceptional capabilities to perceive and respond to external stimuli through programmable alterations in their properties or behaviors. Their unique behavior stems from intrinsic responsiveness to environmental variables, such as temperatures, mechanical stresses, magnetic fields, and chemical environments, enabling adaptive functionalities, including reconfiguration, phase transformation, and controlled reversible actuation [1]. Based on their stimulus-response mechanisms, intelligent metallic materials can be systematically categorized into three primary classes, as illustrated in Figure 1: high-entropy alloys (mechanical/environmental responsiveness), shape-memory alloys (thermal/stress responsiveness), and soft magnetic materials (magnetic field responsiveness).

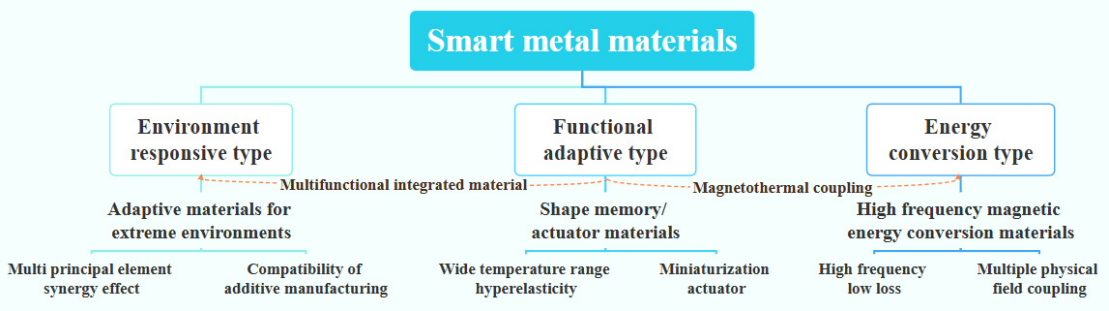

Figure 1. Construction of tree graph for intelligent material classification.

High-entropy alloys (HEAs), characterized by their multi-principal elemental compositions, demonstrate exceptional mechanical properties [2] and corrosion resistance [3] for nuclear-fusion reactors [4], and extreme-environment applications [5]. Shape-memory alloys (SMAs), particularly the emerging high-entropy shape-memory alloys (HESMAs) that synergize HEA-design principles with SMA functionality, achieve shape recovery through thermally induced phase transformations [6]. Soft magnetic materials (SMMs), distinguished by high permeability and low coercivity, form the cornerstone of electromagnetic energy-conversion systems [7]. These materials have driven transformative innovations across aerospace, biomedical, and energy sectors, enabling applications ranging from self-healing aircraft components to stimuli-responsive drug-delivery systems [8–12].

Recent advancements reveal three evolutionary trajectories: Multifunctional integration combines multiple stimulus-response mechanisms within single-material systems, exemplified by HESMAs' dual thermal-stress responsiveness [13]. The process-material synergy leverages additive manufacturing to architect microstructural gradients in HEAs and 4D-printed SMA actuators [2,14,15]. Sustainability-driven development focuses on eco-friendly synthesis methods and lifecycle optimization. This study systematically investigates the intelligent design paradigms of HEAs, SMAs, and SMMs through dual perspectives of material science and processing technology. The materials-science analysis deciphers performance characteristics and domain-specific applications, while the processing-technology section evaluates conventional smelting, Taylor-Ulitovsky methods, and additive manufacturing. This dual-dimensional framework establishes theoretical foundations for next-generation intelligent materials that transcend conventional performance boundaries.

2. Categories and Properties of Smart Materials

2.1. High-Entropy Alloys

2.1.1. Fundamental Concepts and Design Principles

High-entropy alloys (HEAs) are defined as metallic systems containing at least five principal elements (5–35 at.%) [16]. Early research focused on single-phase solid solutions (e.g., Cr-Co-Fe-Mn-Ni FCC systems), while second-generation HEAs relax compositional constraints to allow non-equiatomic and multiphase architectures (Figure 2). This definition primarily emphasizes compositional criteria and yet neglects phase-formation characteristics. An alternative definition requires HEAs to form single-phase solid solutions with equiatomic or near-equiatomic ratios, imposing dual constraints on the phase purity and stoichiometric uniformity. Consequently, the pursuit of single-phase solid solutions with five or more principal elements has dominated the HEA research for decades. Recent advancements have transcended these constraints, with non-equiatomic multiphase HEAs (a matrix being solid solutions) emerging as critical components. This evolution categorizes HEAs into first-generation and second-generation systems [17,18], as illustrated in Figures 2 and 3.

On the isothermal section of a ternary phase diagram, a schematic comparison is presented among: (i) conventional alloys with a dominant base element and minor alloying additions, (ii) equiatomic high-entropy alloys (HEAs) exhibiting uniform elemental distributions, and (iii) non-equiatomic HEAs retaining substantial compositional complexity despite deviating from stoichiometric equivalence. As depicted in Figure 3, the HEA relaxation criteria include non-equiatomic compositions, which have expanded the explorable compositional space and correspondingly accessible material properties [18].

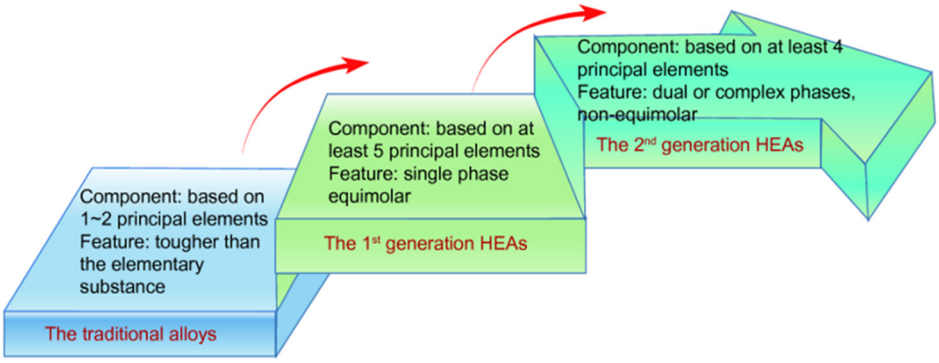

Figure 2. The evolutionary trajectory of alloys illustrates the exponential expansion of a compositional design space from conventional alloys to non-equiatomic HEAs [17].

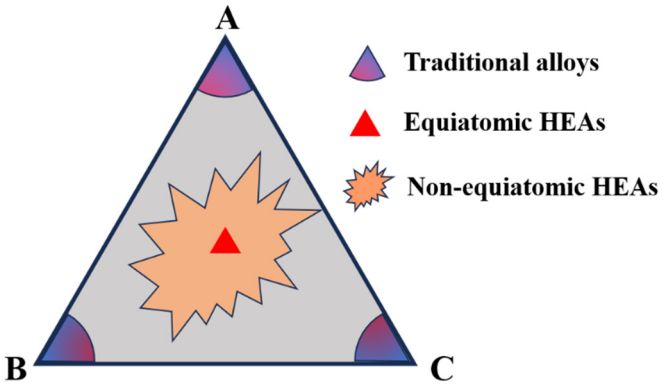

Figure 3. Phase-diagram mapping of equiatomic HEAs, non-equiatomic HEAs, and conventional alloys [18].

Phase engineering stands as the cornerstone for performance optimization in HEAs. Predominant crystal architectures encompass body-centered-cubic (BCC), face-centered-cubic (FCC), and hexagonal-close-packed (HCP) configurations. Targeted phase stabilization is achieved through elemental selection and stoichiometric control. The Cr-Co-Fe-Mn-Ni system predominantly forms FCC structures, whereas the Ti-Zr-Hf-Nb-Ta system favors BCC arrangements [16,19]. Advanced phase-design strategies incorporate nano-precipitates or amorphous phases to enhance mechanical and functional properties.

The intelligent responsiveness of HEAs arises from their metastable states enabled by high configurational entropy. Taking the Ti-Zr-Hf-Ta system as an example, stress-induced martensitic phase transformations exhibit full reversibility through thermal activation, demonstrating superior energy efficiency in two-way memory effects compared to conventional alloys. Under electric field modulation, Fe-Co-Ni-Cr-Mn HEAs exhibit dynamically adaptive passivation behavior, autonomously regulating surface states in electrochemical environments to achieve significant corrosion resistance enhancement.

2.1.2. Property Characteristics

Distinguished from conventional alloys, HEAs leverage their high configurational entropy to form simple solid-solution structures (e.g., FCC, BCC, or HCP), exhibiting superior performance attributes. Their contributions to smart materials are elaborated through three key dimensions:

1. Exceptional Mechanical and Functional Properties

HEAs demonstrate an optimal strength-ductility synergy, maintaining mechanical integrity under extreme conditions—a critical feature for shape-memory alloy matrices. Song et al. [20] fabricated a metastable hypoeutectic $AlCo_{0.4}CrFeNi_{2.7}$ HEA via laser-powder bed fusion (L-PBF), achieving an extraordinary strength-ductility combination. Further annealing treatments increased the tensile yield strength and ultimate strength to 1201 MPa and 1512 MPa, respectively, while maintaining an elongation of ~15.1%. Selected HEAs exhibit exceptional thermal stability and superplasticity at elevated temperatures, enabling their use in temperature- or stress-responsive smart materials. Zhang et al. [21] demonstrated that additive manufacturing induces rapid

cooling, refining grain structures, and forming unique substructures (e.g., cellular architectures), thereby enhancing thermal stability and dynamic responsiveness.

2. Chemical and Electrochemical Attributes

Certain HEAs display outstanding electrocatalytic performance for energy applications, including fuel cells and water splitting. Chang et al. [22] reported a PtPd HEA with record-breaking activity and stability in ethanol-oxidation (EOR) and oxygen-reduction reactions (ORR), achieving a peak power density of 0.72 W cm^{-2} and stable operation over 1200 h in direct ethanol fuel cells (DEFCs). This work establishes a design paradigm for nanostructured alloys in renewable energy systems. The homogeneous microstructure and unique electronic configurations of HEAs confer superior corrosion resistance in harsh environments. Wu et al. [23] attributed the enhanced corrosion resistance of $CoCrFeNiAl_{0.3}$ HEA seamless tubes to reduce the B2-phase content and the formation of a protective passive film enriched with Al, Cr, and Fe.

3. Cross-Disciplinary Smart-Material Applications

Partially HEAs exhibit excellent biological compatibility and wear resistance and can be used as bone implants and smart medical-device materials. Lu et al. [24] developed a TiZrHfTa HEA exhibiting an elastic modulus (29–37 GPa) matching bone tissue and 25% plasticity. Dynamic strengthening via stress-induced martensitic transformation, twinning, and amorphization simultaneously reduces modulus mismatch and enhances crack resistance, with in vitro studies confirming biocompatibility for long-term implantation. HEAs' dual resistance to thermal degradation and corrosion makes them ideal for smart coatings in aerospace and marine systems. Xia et al. [25] demonstrated that incorporating SiC particles into CoCrFeNiCu HEA coatings progressively improves corrosion resistance in 3.5% NaCl solutions, correlating with SiC-induced microstructural refinement.

The evolution from strictly defined first-generation HEAs to second-generation systems incorporating non-equiatomic compositions and multiphase architectures has exponentially expanded their composition-property design space. Breakthroughs in mechanical robustness, electrochemical functionality, and cross-domain adaptability position HEAs as transformative smart material platforms, necessitating further exploration of composition-microstructure synergies for next-generation applications. These advancements, summarized in Table 1, highlight their industrial viability in aerospace impact-resistant structures, nuclear reactor cladding, and seawater electrolysis anodes.

Table 1. Intelligent characteristics and industrial applications examples of HEAs.

Stimulus Type	Response Mechanism	Exemplary Alloys	Performance Enhancement	Application Scenario
Mechanical stress	Dislocation slip inhibits	AlCoCrFeNi [26]	40% strength enhancement	Aerospace impact-resistant structures
High-temperature environment	Self-repair of the oxide layer	CoCrFeMnNi [19]	80% reduction in corrosion rate	Nuclear reactor liner
Electrochemistry field	Passivation film reconstruction	FeCoNiCrCu [25]	Open circuit potential +0.3 V	Seawater electrolysis anode

2.1.3. Research Frontiers

Machine learning (ML) techniques have emerged as transformative tools for accelerating HEA development through composition design and property prediction. By constructing composition-property databases, ML models enable rapid screening of high-performance HEA candidates, dramatically reducing experimental iterations and R&D costs. ML algorithms (random forests, support vector machines, neural networks, etc.) establish composition-property correlations from existing datasets. Rao et al. [27] developed an active learning framework to accelerate HEA design in vast composition spaces using sparse data, particularly for invar-type alloys. The combinatorial complexity of the HEA composition space surpasses traditional experimental capabilities. ML synergizes experimental and computational data to build predictive databases, as demonstrated by Zhang et al. [28] who curated a 5000+ entry HEA database enabling efficient ML-driven screening.

ML-optimization hybrids (genetic algorithms and particle-swarm optimization) enable high-throughput screening. Rickman et al. [29] achieved record-hardness HEAs through genetic algorithm-guided composition optimization. The adoption of ML tools has revolutionized phase diagrams and thermodynamic-property predictions, with Huang et al. [30] demonstrating that neural networks can predict HEA phase stability across multi-component systems.

Despite remarkable progress, critical challenges persist in ML-driven HEA research:

Data Limitations: Current HEA datasets suffer from sparsity and heterogeneity, restricting ML model accuracy [28]. Interpretability Deficit: The black-box nature of advanced ML models hinders physical insights, necessitating explainable AI methods [27]. Multi-Objective Complexity: Concurrent optimization of strength, ductility, and corrosion resistance requires advanced Pareto frontier-exploration techniques [29].

Data Ecosystem Development: Synergizing high-throughput experiments with CALPHAD/MD simulations to expand composition-property databases. Domain-Specific Algorithms: Creating ML architectures tailored for HEA complexity, including graph neural networks for phase prediction. Cross-Disciplinary Convergence: Establishing materials informatics platforms integrating ML experts and metallurgists for accelerated discovery [30].

2.2. Shape-Memory Alloys

2.2.1. Principal Systems

Smart materials exhibit deterministic responses to external stimuli, such as stress and temperature [31]. SMAs are a class of metal materials that can "remember" their initial shape under certain conditions and recover through temperature, mechanical force, or magnetic field changes, with significant intelligent properties. The growing demand for adaptive systems has driven the need for compact sensors, actuators, and microcontrollers. However, conventional solutions often incur undesirable mass-volume penalties, particularly in space-constrained smart applications requiring high functional density, rapid response, and cost-effectiveness [32].

SMA research originated in 1932 with Arne Ölander's discovery of unique thermomechanical properties [33]. The field was revolutionized in 1962 when William Buehler and Frederick Wang identified the shape-memory effect (SME) in NiTi alloys [34,35], establishing them as the benchmark SMA system with broad technological applicability. The discovery of a magnetic-field-induced strain (MFIS) in Ni-Mn-Ga ferromagnetic SMAs by Ullakko [36] catalyzed research on Ni-Mn-X (X = Sn, In, and Sb) systems for magnetocaloric applications, while multi-principal-element SMAs have emerged as a new frontier.

HESMAs require a substitution of base elements with multiple alternatives. Chen et al. [37] demonstrated that $(TiZrHf)_{50}Ni_{25}Co_{10}Cu_{15}$ HESMA maintains SME comparable to $Ti_{50}Ni_{50}$ while achieving a 650 MPa bending stress tolerance and enhanced work output through optimized homogenization. NiMn-based systems like NiMnGaCoCu [38] and NiMnGaCoCuFe [39,40] highlight the criticality of selecting substituents with compatible solubility and electronic configurations. Figure 4 maps equivalent elements across five chemical groups, providing a roadmap for the next-generation SMA design.

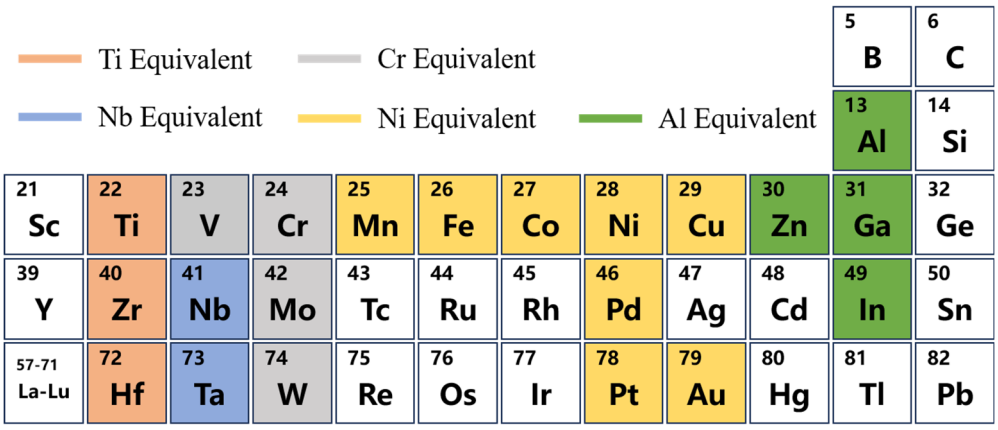

Figure 4. Equivalent elements of five main chemical elements in high-entropy shape-memory alloys.

SMAs permeate diverse sectors from biomedical devices to aerospace actuators [41–43]. While Fe-based (e.g., Fe-Mn-Si) and Cu-based (e.g., Cu-Zn-Al) SMAs offer cost advantages, NiTi systems dominate due to superior thermomechanical stability and cyclic durability. In practical implementation, SMAs demonstrate distinct advantages guided by application-specific requirements, serving as critical enablers for multidisciplinary engineering advancements. SMAs derive their technological significance from SME and superelasticity—the ability to recover original configurations post-thermomechanical deformation. As illustrated in Figure 5, SME manifests as one-way, two-way, or superelastic modes. The reversible microstructure arises from coherent austenite-martensite interfaces, where a lattice misfit generates elastic-stress fields. Strain-energy relaxation occurs via martensite variant twinning/domaining. Hysteresis emerges from asymmetric-forward/reverse-transformation

paths, with stored elastic-energy driving phase reversal. Transformation hysteresis quantifies activation barriers from: (1) Phase boundary motion; (2) Inter-variant friction; (3) Intra-variant twinning resistance; and 4) Phase-defect interactions.

2.2.2. Fundamental Principles and Advanced Applications

SMAs, distinguished by their unique phase-transformation characteristics, contribute to smart-material technologies through three key mechanisms:

1. Memory Effects and Superelasticity

One-way shape-memory effect: Thermally activated restoration of pre-deformed SMAs to their original configuration enables applications in self-repairing structures and micro-actuators. Two-way shape-memory effect: Thermomechanical training protocols allow SMAs to reversibly switch between dual configurations during heating/cooling cycles, facilitating shape-morphing systems and complex motion control. Superelasticity: Near-instantaneous strain recovery (up to 8%) upon stress removal at ambient temperatures makes SMAs ideal for wearable electronics and energy-dissipating systems.

Owing to their macroscopic shape reversibility—namely the SME and superelasticity (SE)—SMAs have found widespread applications in biomedical, automotive, and aerospace industries. Both effects originate from the thermoelastic-martensitic transformation (MT). Consequently, the application domains of SMAs are governed by MT characteristics, including transformation temperatures (TTs), phase-transition pathways, thermal and stress hysteresis (ΔTH and ΔσH), transformation strain, and cyclic stability [43].

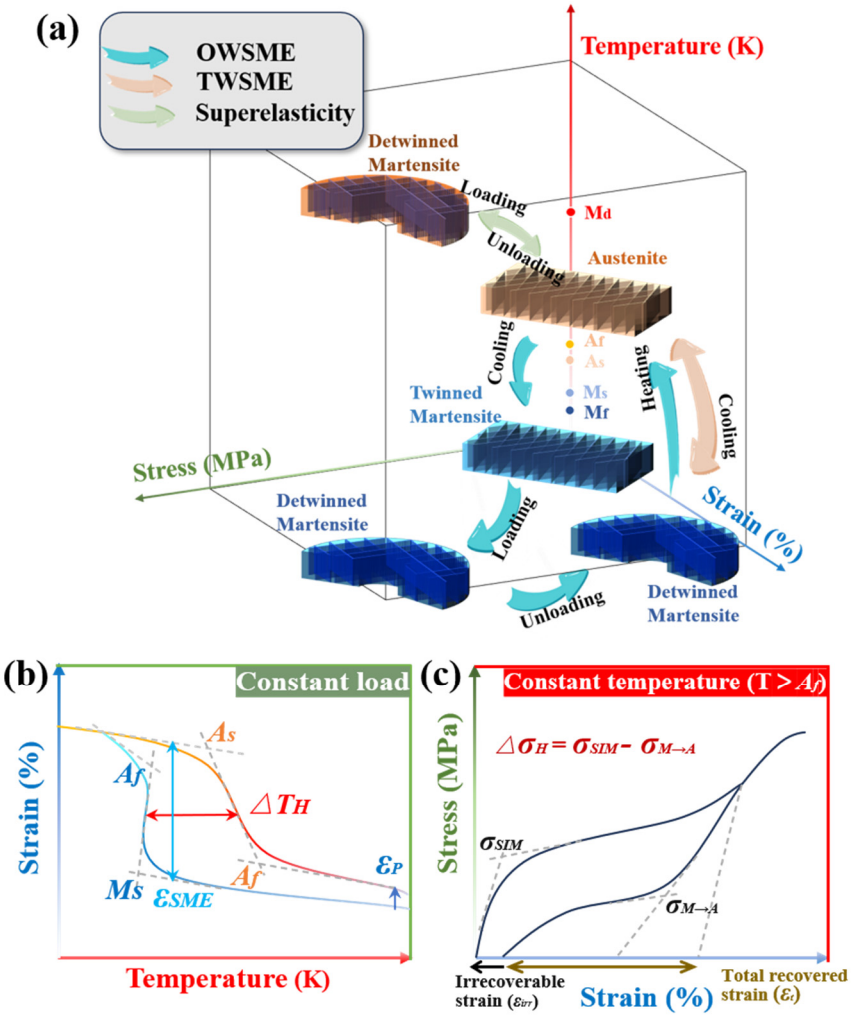

Figure 5. (**a**) Phase and crystal structure of SMA. (**b**) Thermal cycling curves under constant load. (**c**) Stress–strain response at a constant temperature [43].

2. Applications in Smart Actuators

SMAs are widely employed in smart actuators due to their thermally driven capability to generate significant strain and force outputs. Representative applications include: Micro robotic arms [44]: SMA wires serve as core components for micro robotic arms owing to their lightweight nature and high-energy efficiency. Artificial muscles [45]: SMAs mimic the contraction-relaxation behavior of biological muscles, enabling applications in medical assistive devices and robotics.

3. Applications in Sensors and Energy Harvesting

SMAs function as temperature/strain sensors and energy harvesters. Sensors [46]: SME-based sensors monitor temperature variations or stress states for structural health monitoring in spacecraft and civil infrastructures. Energy harvesters [47]: Thermomechanical-energy conversion during phase transitions enables high-efficiency thermal energy harvesting devices.

4. Biomedical Contributions

SMAs' exceptional biocompatibility and responsiveness make them critical materials for medical devices [48]. Stents: NiTi alloys are extensively used in vascular stents and orthopedic implants due to their SME and biocompatibility. Orthodontic devices: Superelastic SMA wires provide sustained, gentle forces for dental alignment. Minimally invasive surgical tools: Temperature-triggered shape adaptation enables complex minimally invasive instruments.

5. Aerospace and Smart-Structural Applications

SMAs' high specific strength, fatigue resistance, and controllability are pivotal in aerospace and structural control [15]. Morphing wing surfaces: Adaptive-wing technologies enhance aerodynamic efficiency through SMA-driven shape control. Vibration dampers: SMA-based dampers absorb/release energy via phase transitions for noise and vibration suppression. Self-healing materials: SMA-enabled smart structures autonomously repair cracks, extending system lifespan.

6. Potential in Wearable Technologies

Smart textiles: SMA-embedded fabrics enable dynamic shape and temperature regulation. Wearable sensors: SME-based motion sensors are applied in health monitoring and sports analytics [49].

2.2.3. Challenges and Improvements

SMAs face two critical challenges in practical applications. 1. Fatigue failure under cyclic loading: Repeated phase transitions and plastic deformation lead to fatigue failure, especially under high-frequency or large-strain conditions, drastically reducing service life. Mechanisms include phase transition-induced microstructural damage [50], thermomechanical-coupling effects [51], and surface defect-driven stress concentration [52]. 2. Multifield coupling effects: In thermoelectromagnetic environments, Joule heating in electro-activated SMAs causes localized overheating [53], while the stress-magnetic field coupling in magnetically controlled SMAs induces nonlinear phase transitions [54]. These challenges constrain long-term reliability and application scope.

To address these challenges, researchers have proposed improvement strategies: Enhancing fatigue resistance: Optimizing compositions (e.g., Cu/Fe doping in Ni-Ti) improves phase-transition behavior [55]; thermomechanical processing refines microstructures to suppress crack initiation [56]; surface treatments (shot peening and laser modification) introduce compressive residual stresses [57]. Optimizing multifield responses: Multiphysics models (e.g., thermomechanical coupling) predict SMA behavior; composition/process tuning enhances performance; intelligent control strategies (adaptive/fuzzy control) mitigate nonlinearities. These advances support broader SMA applications.

2.3. Soft Magnetic Materials

2.3.1. Key Performance Metrics

The quintessential metrics for soft magnetic materials—high permeability (μ), low coercivity (Hc), minimal losses, and high saturation flux density (Bs)—dictate their electromagnetic device performance and application scope. High permeability ($\mu > 10^4$) governs a rapid magnetic response, enhancing energy efficiency by reducing eddy-current losses (>30% improvement vs. conventional steels) [58]. Ultralow coercivity (Hc < 1 A/m in Fe-based amorphous alloys) minimizes hysteresis losses, enabling superior high-frequency (>100 kHz) performance. Core losses (Pcv < 0.1 W/kg at 1 T/50 Hz) in amorphous alloys are 90% lower than silicon steels, revolutionizing

energy-efficient power systems [59]. Breakthrough FeCo-based amorphous-nanocrystalline alloys achieve a record of Bs = 1.94 T, overcoming the 2.0 T theoretical limit for crystalline counterparts [60].

2.3.2. Materials Systems and Design

The design of soft-magnetic material systems primarily focuses on amorphous alloys, nanocrystalline alloys, and high-entropy soft magnetic alloys, each offering distinct performance advantages and application scenarios.

Fe-based amorphous alloys are fabricated via rapid solidification techniques, exhibiting amorphous structures with low coercivity (e.g., ~1 A/m for Fe-Si-B systems) and high resistivity. These alloys are widely employed in power-distribution transformers to minimize energy losses [61,62]. Due to their high permeability, cobalt-based and Fe-Ni-based amorphous alloys are utilized in high-precision applications, such as magnetic shielding [63].

Nanocrystalline alloys (e.g., FINEMET) are synthesized through crystallization annealing of amorphous precursors, achieving grain sizes below 20 nm. This microstructure enables high permeability (e.g., 25,000 for Fe-Si-B-Cu-Nb systems) with low core losses [60]. A Fe-Co-Mo-Cu-Nb-Si-B nanocrystalline alloy developed by the Chinese Academy of Sciences demonstrates a permeability of 36,000 at 100 kHz and a 44% reduction in losses, offering a breakthrough for high-frequency applications [64].

High-entropy soft-magnetic alloys represent an emerging research frontier. Their multi-principal-element design (e.g., Fe-Co-Ni-Cu-Mn) induces lattice-distortion effects, significantly enhancing integrated properties. Although still in the laboratory stage, their potential for high permeability, low losses, and superior mechanical strength has garnered substantial interest. Table 2 summarizes representative soft magnetic-alloy systems with corresponding fabrication methods and magnetic properties.

Table 2. Summary of representative soft-magnetic alloy systems with magnetic properties and fabrication processes.

Material System	Preparation Process	Coercivity H (A/m)	Saturation Magnetization Ms (emu/g)	Magnetic Induction Bs (T)	Initial Magnetic Permeability μ_i (KHz)	Power Loss (kW/m ^{3})	References
$Fe_{79}Ni_1Si_7B_8P_4Cu_1$	Spin strip rapid quenching/annealing (18μm)	2.48	-	1.58	~16,400	-	[65]
$Fe_{85}B_{13.5}Cu_{1.5}$	Single roll melt spinning (22 μm)	35	208 emu/g	-	-	-	[66]
FeSiCrB AMPCs	Aerosolization method/inorganic organic coating	-	-	-	18.6 (16MHz)	489.6 mW/cm^3	[67]
$Fe_{77}Ni_1Si_9B_{13}$	Single-roll spinning melt (25 μ m)	3	-	0.8	-	-	[68]
$Fe_{80}Co_3B_{10}Si_3C_3P_1$	Single-roll rapid quenching method	2.2	-	1.75	30,000	0.11 W/kg	[69]
$Fe_{73.5}Si_{15.5}B_4Cu_1Nb_3P_3$	Single-roll rapid quenching method	0.97	-	-	~10,000	-	[70]
$Fe_{83.3}Si_3B_9P_3Cu_{0.7}C_1$	Single-roll rapid quenching method	6	-	1.65	-	-	[71]
$Fe_{85}B_{10}C_1P_4$	Single-roll rapid quenching method	5.1	165	-	-	-	[72]
$Fe_{82}B_{13}Si_1Cu_1$	Single-roll strip throwing method	4.92	-	1.7	7100	-	[73]

Note: μ_i denotes initial permeability; Pcv refers to volumetric power loss.

2.3.3. Applications and Emerging Trends

Soft magnetic materials demonstrate significant application value across multiple domains due to their high permeability, low coercivity, and minimized energy losses. In the energy sector, Fe-based amorphous alloy transformers reduce core losses by 70% compared to conventional silicon steel transformers [74], substantially enhancing energy efficiency. Under high-frequency conditions (e.g., above 100 kHz), nanocrystalline alloys (e.g., FINEMET) maintain stable permeability, serving as critical materials for on-board chargers (OBCs) and DC/DC converters. Current research prioritizes high-frequency and miniaturization requirements: Nanocrystallization regulation (e.g., Co/Mo doping to induce magnetic-domain nucleation) achieves effective permeability (μ_e) exceeding 36,000 at 100 kHz, while ultra-thin amorphous ribbons (<20 μm) and nanocrystalline films enable integrated micro-inductor fabrication [64]. To overcome the historical trade-off between conflicting properties, amorphous-nanocrystalline transitional alloys [e.g., $(Fe_{0.8}Co_{0.2})_{85}B_{12}Si_2V_{0.5}Cu_{0.5}$] achieve a breakthrough in the

concurrent optimization of saturation-flux density (Bs = 1.94 T) and coercivity (Hc = 4.3 A/m). Meanwhile, machine learning-guided compositional screening is accelerating the intelligent development of next-generation soft-magnetic materials [60].

3. Intelligent-Processing Technologies for Multifunctional Applications

HEAs face a critical research challenge in efficiently screening and designing core compositions due to their vast compositional space. Conventional trial-and-error methods, which fabricate single bulk samples via arc melting, are time-consuming and labor-intensive, hindering the rapid identification of high-performance alloys and optimization of composition-structure-property models. To address this feature, Figure 6 illustrate advanced high-throughput preparation (HTP) technologies: bulk combinatorial-metallurgy screening, laser-additive manufacturing, combinatorial thin-film techniques, diffusion-couple methods, and hot-isostatic pressing (HIP)-enabled micro-synthesis. These approaches drive the HEA discovery and optimization, integrated with machine learning for accelerated data processing. Multifunctional-intelligent processing overcomes traditional manufacturing limitations by integrating sensing, actuation, and adaptive control capabilities. This technology enables complex structural design and functional integration of smart metallic materials (e.g., HEAs, SMAs, and SMMs), aiming to achieve seamless transitions from the "material synthesis" to "device fabrication" via the precise control of microstructures, phase transformation, and functional responses.

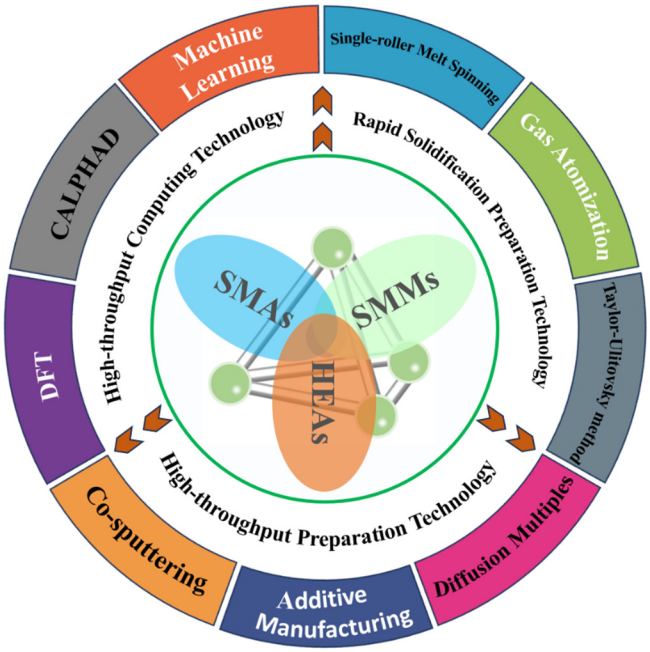

Figure 6. Multifunctional-intelligent processing technologies for smart-metallic materials.

3.1. High-Throughput Preparation of High-Entropy Alloys

HEAs, characterized by their multi-principal-element design (high configurational entropy) and exceptional properties (e.g., high strength, corrosion resistance, thermal stability), have emerged as a research frontier in materials science. However, traditional trial-and-error approaches are inadequate for exploring their vast compositional space. High-throughput preparation (HTP) technologies [75,76] address this gap by enabling parallel synthesis, rapid characterization, and data-driven analysis, significantly accelerating the optimization of composition-process-property relationships. The HTP technologies for HEAs employ diverse methodologies to accelerate composition-structure-property studies. Bulk combinatorial metallurgy (RAP) enables efficient screening via semi-continuous casting, hot/cold rolling, and homogenization, allowing simultaneous synthesis and microstructural analysis of multiple alloys (e.g., Fe-Mn-Ni-Co-Cr systems) in a single experiment. However, limitations include restricted sample numbers (typically ≤ 5) and macro-segregation risks [18,77].

Laser additive manufacturing (LENS) overcomes these limitations using multi-powder nozzles and gradient deposition strategies [78]. It fabricates composite alloy arrays (e.g., $CrCuFeNi_2$-Al gradients) on a single substrate [79], with rapid solidification suppressing segregation. This process allows direct correlation of composition

gradients with phase transitions (e.g., FCC → BCC), though microcracks and precision fluctuations (e.g., ±10% deviation in MoNbTaW systems) remain challenges [80].

Thin-film and diffusion methods focus on microscale exploration: combinatorial thin films (e.g., MnFeCoNiCu systems) are sputter-deposited on silicon wafers to create nanoscale gradients, enabling rapid identification of single-phase compositions (e.g., $Mn_{30}Fe_{20}Co_{22}Ni_{15}Cu_{15}$) [81]. However, they fail to replicate bulk-precipitation behaviors. Diffusion couples construct continuous composition interfaces (e.g., AlCoCrFeNi systems) through high-temperature diffusion, revealing phase-formation kinetics (e.g., B2-A2-FCC layered structures) but constrained by diffusion lengths and sample counts [82].

Emerging HIP microarrays integrate laser-printed honeycomb molds with powder filling (e.g., CoCrNiFe-X systems), enabling simultaneous sintering and evaluation of hundreds of micro-alloys under uniform conditions. This feature enhances compositional diversity and data reliability, establishing a closed-loop validation platform for multi-component alloy design [83].

Each method offers unique strengths: RAP and LENS excel in macroscale screening, thin films and diffusion couples elucidate micromechanisms, while HIP drives miniaturization and integration. Collectively, they advance rational HEA design. Current challenges include composition uniformity control and discrepancies between small-sample and bulk material properties. Future directions involve developing cross-scale processes (e.g., atomic layer deposition combined with 3D printing), integrating active-learning algorithms for experimental optimization, and establishing standardized data-sharing platforms. HTP technologies catalyze a paradigm shift from "quantity" to "quality," offering revolutionary tools to overcome HEA development bottlenecks and accelerate deployment in energy, aerospace, and beyond.

3.2. Data-Driven Design of Intelligent Materials

Intelligent materials (e.g., shape-memory alloys, self-healing polymers, photo-responsive materials) dynamically adapt their properties in response to environmental stimuli (temperature, stress, electromagnetic fields, etc.), demonstrating broad potential in flexible electronics, biomedicine, and energy conversion. However, traditional trial-and-error approaches struggle with multi-physics coupling and cross-scale response challenges. Data-driven smart material design (DDSMD) integrates machine learning, multiscale modeling, and high-throughput experiments to establish an intelligent closed-loop optimization framework spanning "composition-structure-property-response," heralding a new paradigm in materials R&D.

3.2.1. First-Principles Calculations

First-principles calculations for HEAs employ random solid-solution models (e.g., supercells, virtual crystal approximation, coherent potential approximation, and special quasi-disordered supercells) to unravel structure-property relationships in disordered systems. Electronic-structure calculations reveal that chemical and magnetic disorder in 3d HEAs (e.g., CoCrFeMnNi) induces significant broadening of electronic spectral functions near the Fermi level. Paramagnetic-state simulations combined with spin-polarized calculations elucidate the role of local magnetic moments in stability [84]. Phase-stability analysis demonstrates that vibrational entropy dominates Gibbs free energy, favoring FCC structures in the CoCrFeMnNi at elevated temperatures, while the Al addition triggers FCC→BCC transitions. Elastic constant predictions (e.g., Young's modulus of 218.6 GPa for the CoCrFeMnNi) align with experiments, and stacking-fault-energy calculations confirm low faulting tendencies as the key to enhanced ductility [85,86]. Molecular-dynamics simulations quantify lattice distortions (static/dynamic disorder) and sluggish diffusion effects, revealing interstitial diffusion coefficients in NiCoCr, 1–2 orders of magnitude lower than pure metals [87]. While challenges persist in multi-component modeling and temperature coupling, advances in non-local coherent potential approximations and machine-learned interatomic potentials are bridging empirical exploration to predictive design.

3.2.2. CALPHAD Phase-Diagram Modeling

CALPHAD (CALculation of PHAse Diagrams), a cornerstone of data-driven materials design, addresses the complexity of multi-principal-element phase prediction in HEAs through integrated multiscale thermodynamics and machine learning. Traditional CALPHAD frameworks for binary/ternary systems require re-engineered thermodynamic databases incorporating lattice distortions and magnetic entropy for 5–6 component HEAs [88]. For instance, CoCrFeMnNi phase-boundary predictions achieve < 5% deviation (vs. >15% previously) by integrating magnetic-entropy corrections and local strain models, validated via first-principles ΔHmix and experimental activity coefficients [89]. Machine learning enhances HEA phase-design efficiency. Random forest (RF) algorithms identify key descriptors (ΔHmix, atomic-size difference, δ, and valence electron concentration,

VEC) to define phase- stability boundaries: single-phase solid solutions dominate when ΔHmix = −15–5 kJ/mol and δ < 6.5%, while intermetallic/amorphous phases compete beyond these thresholds. Active learning algorithms in Co-Cr-Fe-Mn-Ni systems optimize the CALPHAD efficiency by 3–5 times and reduce experimental validation samples by 70%. For AlxCoCrFeNi alloys, backpropagation neural networks [90] predict x = 0.5 as the FCC/BCC dual-phase critical point, achieving < 8% error in strength-ductility matching.

The closed-loop validation from theory to application highlights the potential of CALPHAD-machine learning synergy. In the Al-Co-Cr-Fe-Ni system, phase diagram calculations delineate dual-phase boundaries and reveal the B2 phase precipitation mechanism induced by Al segregation via lattice dynamics simulations, guiding aging treatments to suppress brittle-phase formation. Integrating quantum-computed electronic structure data with phase-field dynamics simulations will enable cross-scale predictions spanning atomic interactions to macroscopic-microstructure evolution, advancing the HEA design from the empirical trial-and-error to an intelligent "virtual reality" paradigm. This paradigm shift extends beyond alloy development, offering novel pathways for efficient design of fuel-cell catalysts, nuclear cladding materials, and other multi-component systems.

3.2.3. Machine-Learning-Driven Design of High-Entropy Alloys

The deep integration of machine learning (ML) and physics-based modeling is revolutionizing the HEA research. Rao et al. [27] developed an active-learning framework that transcends traditional trial-and-error approaches. Their HEA-GAD (Generative Adversarial Design) system synergizes generative models with ensemble predictors to intelligently explore compositional spaces. The framework first generates candidate compositions, then filters, and optimizes them using a dual-model system (multilayer perception and gradient-boosted decision trees). An experimental-validation feedback loop creates a dynamic "predict-validate-iterate" cycle. Notably, it innovatively integrates solid-solution strengthening theory with explainable ML through a two-stage feature selection strategy, enhancing prediction accuracy for AlCoCrCuFeNi system compositions while providing new insights into physical performance mechanisms.

ML-enhanced atomic-scale simulations demonstrate unique advantages in a catalysis-oriented HEA design. In HEA-PdNiRuIrRh catalyst studies [91], ML-guided Monte Carlo simulations deciphered the correlation between complex surface atomic arrangements and catalytic active sites, uncovering synergistic effects of Pd-Pd-Ni bonding environments and Ni/Ru oxyphilic sites on alkaline-hydrogen oxidation. This atomic-level mechanistic insight enables targeted catalytic performance tuning. The developed ML potential models are transferrable to other multi-component catalytic systems [92,93]. Concurrently, an ML workflow for shape-memory alloys combines feature engineering with the SHAP explainability analysis, achieving precise phase-transition temperature predictions (error < 3%) for TiZrHfNiCoCu systems and identifying critical roles of electronegativity parameter, CV22, and Co/Cu content, providing quantitative guidelines for composition optimization [94].

In process optimization, ML demonstrates robust capabilities in modeling complex manufacturing conditions. A flow-behavior-prediction model integrating random forests and artificial neural networks digitally reconstructed the processing map for CoCrFeNiTa0.395 eutectic HEAs. Remarkably, this model maintains high accuracy (R^2 > 0.99) while experimentally validating correlations between processing parameters and microstructural evolutions, drastically reducing development cycles [95].

These case studies collectively validate ML's universal value in the HEA research: from the composition design to performance prediction and process optimization. ML provides an intelligent end-to-end solution, offering new pathways to overcome the "curse of dimensionality" in multi-component materials.

3.2.4. Future Directions

Current limitations include model generalizability with small datasets, trade-off quantification in multi-objective optimization, and discrepancies between simulated and real-world material responses. Future directions focus on:

Self-Driving Labs: Integrating AI decision-making, robotic synthesis, and real-time characterization for autonomous "design-to-validation" workflows.

Material-Digital Twins: Developing multiphysics-coupled virtual replicas to simulate material behavior under extreme conditions.

Explainable AI: Physics-constrained neural networks bridging data-driven and mechanistic models, transitioning from "black-box" predictions to transparent design.

Data-driven design shifts materials R&D from empirical approaches to knowledge emergence, accelerating intelligent-material deployment and enabling on-demand functional customization.

3.3. Rapid Solidification for Soft Magnetic Materials

A rapid-solidification technology suppresses atomic diffusion via ultrahigh cooling rates (10^5–10^8 K/s), forming amorphous, nanocrystalline, or metastable phases. This process significantly enhances saturation magnetization (Ms) and reduces coercivity (Hc) in soft magnetic materials. Table 3 shows the comparison of three representative preparation methods:

Table 3. Comparison of rapid-solidification techniques for soft magnetic materials.

Method	Cooling Rate (K/s)	Typical Products	Key Performance Indicators	Application Scenarios
Gas Atomization [96]	10^5–10^6	Amorphous/nanocrystalline powders	Ms = 1.2–1.8 T, Hc < 50 A/m	3D printed magnetic cores and inductive components
Taylor-Ulitovsky Process [38]	10^6–10^7	Glass-coated wire	Hc < 2 A/m, Frequency response > 1 MHz	Micro sensors, high-frequency magnetic heads
Melt Spinning [68]	10^6–10^8	Amorphous strip	Loss < 0.2 W/kg (@ 1 T, 1 kHz)	Power transformers, magnetic shielding materials

3.3.1. Gas Atomization

The gas-atomization process utilizes high-pressure inert gas (e.g., Ar, N_2) to disintegrate molten metal streams into micron-sized droplets (Figure 7). Rapid cooling (10^5–10^6 K/s) suppresses grain growth, yielding spherical metallic powders [97]. During flight cooling, droplets experience extreme thermal gradients (>10^6 K/m), stabilizing amorphous/nanocrystalline structures. For instance, Fe-Si-B-alloy droplets solidify into amorphous precursors at 10^6 K/s, providing a foundation for subsequent nanocrystallization annealing [98].

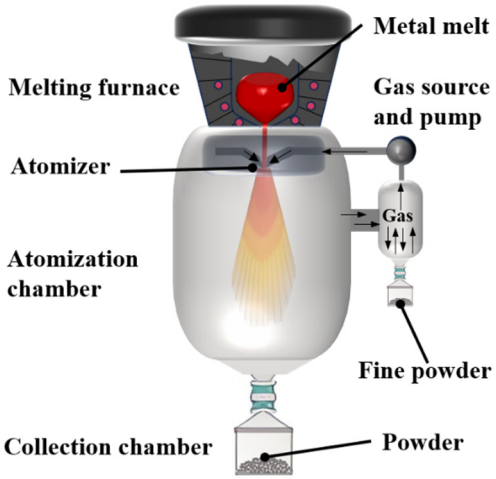

Figure 7. Schematic diagram of atomization-powder production [96].

Key advantages include versatility in powder production. By adjusting gas pressure (3–8 MPa) and melt superheat (200–300 °C), Fe-Co-Nb-B [98] and Fe-Si-B [99,100] powders achieve controlled particle sizes (10–100 μm) with oxygen content < 200 ppm, outperforming conventional water atomization. Post-annealing (e.g., 550 °C/1 h) induces uniform nanocrystallization (grain size of ~20 nm). $Fe_{73.5}Si_{13.5}B_9Cu_1Nb_3$ alloy exhibits Ms = 1.5 T and Hc < 10 A/m, demonstrating superior high-frequency performance [101].

Challenges include high capital costs (e.g., alumina nozzles and gas-recycling systems) and post-processing complexity. High porosity (~30%) necessitates densification via HIP (1000 °C/150 MPa) or SPS (rapid heating to 900 °C), increasing overall costs. Future integration of plasma-assisted atomization (cooling rates up to 10^7 K/s) and in-situ oxygen reduction (<50 ppm) may overcome cost-performance trade-offs.

3.3.2. Taylor-Ulitovsky Process for Glass-Coated Wires

The Taylor-Ulitovsky process co-draws molten metal cores (e.g., Fe-Ni alloys) with glass coatings (e.g., SiO_2) under rapid cooling (10^6–10^7K/s), as shown in Figure 8 [102]. This process forms amorphous/nanocrystalline

composite structures, where 50–200 nm nanocrystals are embedded in an amorphous matrix [103]. $Fe_{40}Ni_{38}Mo_4B_{18}$ wires cooled at 10^7 K/s exhibit γ-Fe(Ni,Mo) nanocrystals (<5 nm), achieving Hc < 0.5 A/m due to oxygen isolation (<50 ppm) and interfacial stress engineering [104].

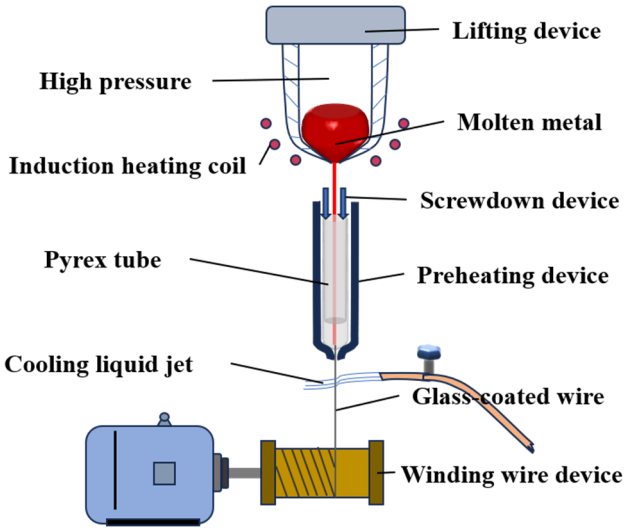

Figure 8. Schematic diagram of Taylor-Ulitovsky Process.

The core advantage of this technology lies in its groundbreaking integration of miniaturization and high-frequency performance. The glass cladding, leveraging chemical stability and insulation properties, enables metal-wire-diameter reduction to 10 μm-scale while maintaining surface roughness of Ra < 0.1 μm, laying the foundation for precision winding of micro-magnetic sensor coils. The amorphous/nanocrystalline composite core structure retains permeability stability (μ′ ≥1000 @1 MHz) in the MHz-frequency range, far surpassing traditional crystalline permalloy (μ′ < 300). These characteristics make it ideal for MRI-compatible coils in implantable medical devices and 5G high-frequency inductors, achieving a 5-fold volume reduction compared to conventional solutions.

However, process-control challenges and interfacial reliability remain key industrialization bottlenecks. The coefficient of thermal-expansion (CTE) mismatch between the glass and metal (e.g., borosilicate glass CTE ≈ 3.3 × 10^{-6}/K vs. Fe-Ni alloy CTE ≈ 8 × 10^{-6}/K) generates interfacial residual stresses up to 200 MPa during cooling, triggering microcracks or delamination. Additionally, the narrow processing window for wire drawing speeds (20–50 m/s) and temperature gradients (>10^7 K/m) limits yield rates below 60%. Future development of gradient transition layers (e.g., metal-glass compositional gradation) and adaptive cooling systems (dynamic-gas-cooling modulation) could reduce interfacial defect rates to <5%, facilitating penetration into cutting-edge fields, such as brain-computer interfaces (BCI) ultra-fine guidewires.

3.3.3. Melt Spinning

The essence of melt spinning lies in its ultra-rapid cooling to achieve non-equilibrium transitions from liquid to solid states. The process involves ejecting molten metal streams (e.g., Fe-Si-B alloys) at controlled flow rates (0.5–2 m/s) onto a high-speed rotating copper roller (linear velocity 20–50 m/s), as shown in Figure 9. Upon contact, a continuous ribbon with a thickness of 20–50 μm forms. The roller's rapid heat extraction (cooling rate 10^6–10^8 K/s) freezes atomic arrangements before crystallization, resulting in amorphous structures [62,105]. The liquid-metal-to-roller contact time (~10^{-4} s) enables quenching from 1500 °C to room temperature under a temperature gradient of ~10^7 K/m. For instance, the $Fe_{78}Si_9B_{13}$ alloy achieves >98% amorphization under these conditions, providing a foundation for nanocrystallization control [106].

An important strength of this technology is its efficiency in producing high-performance soft-magnetic materials. By adjusting roller speed (cooling rate) and melt superheat (ΔT = 200–300 °C), uniform amorphous ribbons are obtained. For example, Fe-Si-B ribbons exhibit a saturation magnetization (Ms) of 1.6 T and 80% lower core losses at 50 Hz compared to conventional silicon steels. Crucially, gradient annealing (e.g., 540 °C/1 h + 380 °C/30 min.) precipitates α-Fe(Si) grains (10–30 nm) in the amorphous matrix, forming a dual-phase structure. The nanocrystalline phase enhances permeability (initial μ > 80,000), while the amorphous phase retains low coercivity (Hc < 3 A/m), optimizing high-frequency loss and magnetic induction [65]. Ma et al. [107] synthesized micrometer-scale fibers (SMFs) with an exceptional strength-flexibility synergy in Fe-Co-Ni-Al-Ta

HEA s via silicon microalloying. Grain coarsening in $Fe_{34}Co_{29}Ni_{29}Al_3Ta_3Si_2$ HEAs, containing coherent nanoprecipitates with low lattice mismatch, induced dislocation-pinning effects for enhanced strength.

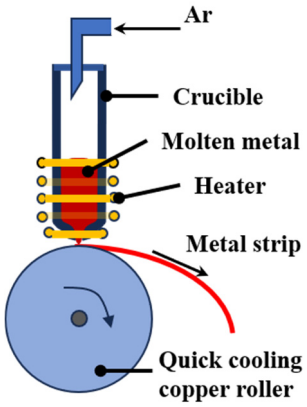

Figure 9. Schematic diagram of Melt Spinning.

However, scalability faces physical and technical limitations. Ribbon width is constrained to < 50 mm due to a copper roller size and thermal load, insufficient for large power transformer cores. Residual stresses (200–500 MPa) from rapid quenching reduce bending toughness, causing edge cracking (defect rate > 5%) during lamination. Current research focuses on multi-roll cooperative jetting (width ≥ 150 mm) and laser-assisted stress relief (60% residual-stress reduction) to overcome brittleness and dimensional constraints.

4. Comparative Analysis and Synergistic Potential

4.1. Performance Comparison

HEAs, SMAs, and SMMs exhibit distinct characteristics in mechanical properties, environmental adaptability, and response speed. Mechanical Strength: HEAs demonstrate ultrahigh-temperature compressive strength (288 MPa at 1800 °C) via multi-principal solid-solution strengthening and synergistic nanoprecipitates (e.g., Nb-Mo-Ta-W-Hf-N alloys), outperforming conventional superalloys. Ni-Ti-based SMAs exhibit a ~600 MPa yield strength but limited fatigue life (10^4 cycles), requiring nanoscale precipitates to improve reliability to 10^5 cycles. Fe-Co-based high-entropy SMMs achieve a breakthrough in yield strength (952 MPa) while retaining high ductility and low coercivity (27 Oe), enabling synergistic mechanical-magnetic performance.

Environmental Adaptability: HEAs excel in high-temperature resistance (>1650 °C) and corrosion tolerance via high-entropy effects, making them ideal for extreme environments (e.g., aerospace turbine blades). SMAs maintain superelasticity across a broad temperature range (−100 °C to 200 °C) but suffer from oxidative degradation at elevated temperatures, necessitating protective coatings. Traditional amorphous SMMs show low magnetic losses at 100 kHz but poor thermal stability. In contrast, high-entropy SMMs with multi-component design (e.g., Mo doping) enhance thermal tolerance to 800 °C, expanding high-temperature/high-frequency applications.

Response Speed: SMAs show varied actuation speeds: thermal actuation requires 1–10 s, while electrical actuation achieves millisecond-level responses but demands high current densities (>10^5 A/cm^2). SMMs surpass traditional silicon steels in inductors due to microsecond-scale magnetic response and stable permeability at 100 kHz. Though lacking intrinsic responsiveness, HEAs' robust matrices serve as multifunctional platforms for integrating piezoelectric or magnetostrictive materials, enabling structural-functional synergy and novel smart-material systems.

4.2. Complementarity in Application Scenarios

HEAs, SMAs, and SMMs form a complementary "structure-actuation-function" system in engineering applications. As structural materials, HEAs are the cornerstone for high-temperature load-bearing components (e.g., aerospace-turbine blades and nuclear-reactor vessels) due to their exceptional thermal resistance and extreme-environment durability. For instance, gradient-designed spacecraft shielding layers (e.g., FeCoNiCr/Al multilayers) optimize energy-absorption efficiency while maintaining structural integrity under intense impacts [26]. SMAs revolutionize biomedical and soft robotics fields via their unique SME. For example, Ni-Ti alloy stents achieve minimally invasive-implantation through body temperature-triggered self-expansion [108], while wide-

temperature-range Ti-Zr-Hf-Ni-Cu alloys enable high-precision actuation (strain recovery > 95%) in flexible robotic joints [109]. SMMs drive functional breakthroughs in energy and electronics. Amorphous-alloy transformers reduce core losses by 70% compared to silicon steels, enhancing grid efficiency, while nanocrystalline soft-magnetic materials (e.g., FINEMET) sustain permeability over 36,000 at 100 kHz, serving as core components for high-frequency devices like on-board chargers [110].

Synergistic design of these materials pushes the performance boundaries of composite systems. In spacecraft thermal protection systems, HEAs provide high-temperature structural support, integrated SMMs sensors monitor deformation and heat flux in real time, and SMA actuators dynamically adjust a surface morphology to optimize heat dissipation, forming a closed-loop "sense-respond-actuate" mechanism. Such cross-material coupling enhances component reliability and enables system-level intelligence through modular integration: HEAs ensure mechanical robustness, SMAs deliver active actuation, and SMMs facilitate energy conversion and signal transmission, collectively building adaptive engineering systems for extreme environments.

The division and collaboration of these materials reflect modern engineering demands for multidimensional performance: HEAs address structural challenges ("how to be stronger and tougher"), SMAs respond to actuation needs ("how to adapt autonomously"), and SMMs solve functional problems ("how to convert efficiently"). Future integration via cross-scale interfacial design (e.g., HEAs/SMMs heterostructures) and multiphysics coupling (thermo-magneto-mechanical synergy) will catalyze next-generation smart-material systems, such as self-sensing anti-impact armor, reconfigurable space manipulators, or lossless wireless charging platforms, advancing aerospace, biomedicine, and energy technologies toward higher integration and autonomy.

4.3. Cross-Innovation Directions

The cross-system integration of HEA-based soft-magnetic materials (HEA-SMMs) and SMA/SMM composites facilitate the transformation of smart device into new dimensions. HEA-SMMs surpass conventional soft-magnetic materials via multi-principal synergy (e.g., Fe-Co-Ni-Cu-Al-Mo systems), achieving compressive strength > 950 MPa while maintaining high saturation magnetization (169.86 emu/g). These materials offer robust, magnetic-reliable solutions for extreme applications like aerospace motor rotors. However, magnetic performance degradation from a reduced Fe/Co content requires balancing through lattice distortion control and elemental ratio optimization. SMA/SMM composite devices pioneer actuation-sensing synergy: Magnetothermal coupling designs leverage eddy-current heating from SMMs under high-frequency fields to trigger SMA-phase transitions, enabling contactless actuation of micro-valves. Embedding magnetoresistive films in SMA actuators allows real-time deformation feedback via magnetic signals, achieving micrometer-level control precision for applications like precision-medical robotic arms.

Multi-material additive manufacturing revolutionizes these hybrid systems. Selective laser melting (SLM) enables microscale interweaving of HEAs, SMAs, and SMMs through layer-wise printing. For instance, in spacecraft sensor-actuator modules, HEA frameworks bear structural loads, SMAs drive deformation, and SMMs convert energy and transmit signals simultaneously. Layer-wise metallurgical bonding reduces interfacial defects, increasing fatigue life by > 3 times. This breakthrough addresses hetero-material compatibility while enabling a digital composition-structure-function design for customizable smart devices.

Future cross-material designs will focus on energy-loop closure and adaptive evolution: HEA-SMMs could serve as magneto-mechanical conversion cores in self-powered systems, SMA/SMMs may form self-sensing/healing networks, and multi-material additive manufacturing will enable rapid responses for in-space manufacturing. For example, deep-space probes could in situ print HEA-SMMs/SMA joints to dynamically adjust magnetic stiffness and shape-memory thresholds, adapting to unknown environmental loads—heralding a transition from static-functional stacking to dynamic-intelligent symbiosis.

5. Challenges and Future Directions

5.1. Technical Bottlenecks

The large-scale application of intelligent-metallic materials remains constrained by critical technical challenges. While the multi-component design of HEAs confers exceptional properties, their mass production faces cost and complexity barriers: Refractory HEAs (e.g., Mo-W-Ta-Nb systems) require energy-intensive laser additive manufacturing under inert atmospheres, with per-unit costs 3–5 times higher than conventional alloys. Rapid solidification of multi-principal melts also induces elemental segregation, necessitating novel homogenization techniques (e.g., electromagnetic stirring coupled with directional solidification) to balance performance and cost efficiency [111]. The functional stability of SMAs is compromised by the micro-damage

accumulation under cyclic loading. Ni-Ti alloys exhibit a 5–8% residual strain after 10^4 thermomechanical cycles, while high-temperature oxidation accelerates phase-boundary degradation. Solutions like nanoscale composite strengthening (TiC doping) or anti-oxidation coatings (Al_2O_3/TiN multilayers) are critical to extend service life [112].

Soft-magnetic materials (SMMs) face high-frequency energy-loss challenges: Conventional Fe-Si-B amorphous alloys reduce core losses by 70% vs. silicon steels at 100 kHz but suffer exponential permeability decay. High-entropy SMMs (e.g., Fe-Co-Ni-Cu-Al) suppress domain-wall hysteresis via multi-component design, and yet lattice distortion-induced domain pinning increases coercivity by 30–50%, exacerbating eddy-current losses [113]. Resolving this issue requires atomic-scale control of magnetic anisotropy—e.g., field annealing for nanocrystalline textures or topochemical synthesis of low-distortion metastable phases. Overcoming these challenges will pave the way for the widespread use of smart materials in high-end sectors like renewable energy and aerospace.

The critical challenges in transitioning from laboratory research to industrial implementation involve reducing HEAs' raw material costs (currently 3–5× higher than conventional alloys) through multi-source scrap alloying with 92% aerospace scrap recycling efficiency, extending SMAs' fatigue life from $<10^4$ to $>10^5$ cycles via nano-precipitate regulation, and addressing SMMs' high-frequency losses using magnetic domain engineering exemplified by Fe-Si-B-Nb-Cu systems achieving 0.11 W/kg loss at 100 kHz. This progress is evidenced by Tesla Model 3's adoption of Fe-Co-Ni-Cu-Al soft magnetic composites, delivering 17% higher energy efficiency than silicon steel in drive motors.

5.2. Emerging Applications

Cross-domain innovations are redefining technological frontiers. In flexible electronics, ultrathin amorphous SMM films (<20 μm) integrated with SMAs enable adaptive devices: A foldable magnetic-field sensor uses Ni-Ti bending to modulate sensitivity, while self-healing circuits with Ag-HEA hybrid wires retain >95% signal fidelity after 10^4 bending cycles—critical for wearable health monitors and soft robotics [114]. Such devices synchronize mechanical deformation, electromagnetic sensing, and energy transfer, transcending rigid electronics' limitations.

Self-healing smart materials excel in extreme environments. HEA composites with dynamic Diels-Alder bonds form 3D reversible networks, achieving > 92% microcrack healing at 120 °C. Combined with a SMA-driven pre-stress, they actively close millimeter-scale damage—e.g., spacecraft shields autonomously repair micrometeoroid impacts via SMA phase transitions and molecular-level bond reformation under thermal radiation, tripling an impact-resistance lifespan. This integrated design marks a leap from passive protection to active self-repair.

In space exploration, smart materials enable multifunctional synergy. Additively manufactured Ti-Zr-Hf-Ni-Cu SMAs retain a >90% strain recovery across −100 °C to 200 °C, powering Mars rover sampling arms. Concurrently, Fe-Co-Ni-Cu-Al-Mo high-entropy SMMs maintain permeability stability (μ > 5000 @100 kHz) under intense radiation, serving dual roles in electromagnetic shielding and wireless power transfer. These space-qualified materials inspire lightweight, intelligent extraterrestrial systems and novel paradigms for an extreme-environment multifield material design.

6. Conclusions

(1) Breakthroughs in High-Performance Materials:

High-entropy alloys (HEAs) achieve extreme-environment mechanical performance through multi-principal solid-solution strengthening and additive-manufacturing synergy. CrCoNi-based alloys exhibit a yield strength exceeding 1.2 GPa with creep resistance across −196 °C to 1000 °C, positioning them as core materials for deep-space exploration structural components. Shape-memory alloys (SMAs) revolutionize medical applications via broad-temperature superelasticity (elastic strain ≥ 8%) and micro-actuation capabilities, exemplified by Ni-Ti stents adapting to vascular morphology and Ti-Zr-Hf-Ni-Cu robotic hands achieving submillimeter precision. Soft-magnetic materials (SMMs) enhance energy efficiency (e.g., 92% wireless-charging efficiency in EVs) and extreme-environment adaptability (e.g., low-loss magnetic confinement in fusion reactors) through nanocrystallization and high-entropy design, such as Fe-Si-B-Nb-Cu systems with permeability exceeding 50,000 @100 kHz.

(2) Multidimensional Synergistic Innovations:

Future materials development should focus on the multifunctional integration and intelligent synthesis: HEA-based soft magnetic composites (e.g., Fe-Co-Ni-Cr-Mo/B) enable structural-functional unity, such as spacecraft

thermal-protection layers combining 2000 °C heat resistance with stress monitoring. SMA/SMM heterojunction actuators (e.g., Ni-Ti/Fe-Ga) achieve millisecond-level response and strain feedback via magnetothermal coupling, advancing biomimetic actuation in brain-computer interfaces. Intelligent-manufacturing technologies (e.g., digital twins optimizing multi-material interfacial strength to 85%, machine- learning reducing SMA development cycles from 5 years to 6 months) accelerate the material-to-device translation, meeting emerging demands like in-space manufacturing.

(3) Cross-Disciplinary Paradigm Shift:

Materials science converges with AI and quantum computing, establishing an innovation chain from "atomic simulation to multiscale manufacturing to system integration": Molecular dynamics guide the HEA grain-boundary segregation control, while a magnetic-domain topology optimizes SMM high-frequency response. Multi-material additive manufacturing fabricates HEA/SMA/SMM hybrid spacecraft modules, while green technologies (recyclable HEAs, low-energy SMA actuators) build sustainable ecosystems. This "sense-respond-evolve" intelligent material paradigm will drive breakthroughs in deep-sea/space exploration and carbon neutrality.

Author Contributions

R.L.: Led the core conceptual design and methodology development, managed experimental data, and drafted the manuscript. P.K.L.: Provided critical validation of results, secured resources (e.g., materials, equipment), and contributed to manuscript revisions. J.J.: Conducted detailed data analysis, experimental investigations, and visualization of results. Y.Z.: Oversaw the project, coordinated funding, and finalized the manuscript through rigorous editing. All authors have read and agreed to the published version of the manuscript.

Funding

Financial support from the National Natural Science Foundation of China (52371165 and 12275237), the Department of Science and Technology of Fuzhou city (2024-Y-017, 2024-SG-003 and 2024-SG-004), the Key Laboratory of Silicon-based Materials, The Ministry of Education, P. R. China, the Key Laboratory of Silicon-based Materials, The Ministry of Education, P. R. China, the Key Laboratory of Automotive Glass of Fujian, the Smart Automotive Glass Engineering Research Center of Fujian, the Space Application System of China Manned Space Program (KJZ-YY-NCL09) and China-ESA international cooperation (KF-2020-68) are gratefully acknowledged. PKL very much appreciates the support of (1) the National Science Foundation (DMR-1611180, 1809640, and 2226508), (2) the Army Research Office Project (W911NF-13-1-0438 and W911NF-19-2-0049), (3) the Department of Energy (DOE DE-EE0011185), and (4) the Air Force Office of Scientific Research (AF AFOSR-FA9550-23-1-0503).

Institutional Review Board Statement

Not applicable.

Informed Consent Statement

Not applicable.

Data Availability Statement

The datasets generated and analyzed during the current study are available from the corresponding author upon reasonable request. The data will be retained for at least 10 years following publication through institutional archives or subject-specific repositories, with access restrictions applied only to protect participant confidentiality or proprietary rights.

Conflicts of Interest

The authors declare no conflict of interest. The funders had no role in the design of the study; in the collection, analyses, or interpretation of data; in the writing of the manuscript; or in the decision to publish the results.

References

1. Guan, Q.; Fang, Y.; Wu, X.; et al. Stimuli responsive metal organic framework materials towards advanced smart

application. *Mater. Today* **2023**, *64*, 138–164. https://doi.org/10.1016/j.mattod.2023.02.013.
2. Ren, J.; Zhang, Y.; Zhao, D.; et al. Strong yet ductile nanolamellar high-entropy alloys by additive manufacturing. *Nature* **2022**, *608*, 62–68. https://doi.org/10.1038/s41586-022-04914-8.
3. Li, T.; Wang, D.; Zhang, S.; et al. Corrosion Behavior of High Entropy Alloys and Their Application in the Nuclear Industry—An Overview. *Metals* **2023**, *13*, 363. https://doi.org/10.3390/met13020363.
4. Barron, P.J.; Carruthers, A.W.; Fellowes, J.W.; et al. Towards V-based high-entropy alloys for nuclear fusion applications. *Scr. Mater.* **2020**, *176*, 12–16. https://doi.org/10.1016/j.scriptamat.2019.09.028.
5. Wang, X.; Huang, H.; Shi, J.; et al. Recent progress of tungsten-based high-entropy alloys in nuclear fusion. *Tungsten* **2021**, *3*, 143–160. https://doi.org/10.1007/s42864-021-00092-8.
6. Jeong, U.; Yin, Y. Smart and Responsive Micro- and Nanostructured Materials. *Adv. Funct. Mater.* **2020**, *30*, 1907059. https://doi.org/10.1002/adfm.201907059.
7. Silveyra, J.M.; Ferrara, E.; Huber, D.L.; et al. Soft magnetic materials for a sustainable and electrified world. *Science* **2018**, *362*, eaao0195. https://doi.org/10.1126/science.aao0195.
8. Keshav, S.; Srinivas, G. Flying smart: Smart materials used in aviation industry. *Mater. Today Proc.* **2020**, *27*, 244–250. https://doi.org/10.1016/j.matpr.2019.10.115.
9. Kim, H.; Ahn, S.K.; Mackie, D.M.; et al. Shape morphing smart 3D actuator materials for micro soft robot. *Mater. Today* **2020**, *41*, 243–269. https://doi.org/10.1016/j.mattod.2020.06.005.
10. Zheng, Y.; Tang, N.; Omar, R.; et al. Smart Materials Enabled with Artificial Intelligence for Healthcare Wearables. *Adv. Funct. Mater.* **2021**, *31*, 2105482. https://doi.org/10.1002/adfm.202105482.
11. Khan, A.; Haque, M.N.; Kabiraz, D.C.; et al. A review on advanced nanocomposites materials based smart textile biosensor for healthcare monitoring from human sweat. *Sens. Actuators A Phys.* **2023**, *350*, 114093. https://doi.org/10.1016/j.sna.2022.114093.
12. Duan, Y.; Liu, K.; Qi, J.; et al. Engineering lignocellulose-based composites for advanced structural materials. *Ind. Crops Prod.* **2023**, *205*, 117562. https://doi.org/10.1016/j.indcrop.2023.117562.
13. Han, L.; Zhu, S.; Rao, Z.; et al. Multifunctional high-entropy materials. *Nat. Rev. Mater.* **2024**, *9*, 846–865. https://doi.org/10.1038/s41578-024-00720-y.
14. Lee, H.T.; Seichepine, F.; Yang, G.Z. Microtentacle Actuators Based on Shape Memory Alloy Smart Soft Composite. *Adv. Funct. Mater.* **2020**, *30*, 2002510. https://doi.org/10.1002/adfm.202002510.
15. Kim, M.S.; Heo, J.K.; Rodrigue, H.; et al. Shape Memory Alloy (SMA) Actuators: The Role of Material, Form, and Scaling Effects. *Adv. Mater.* **2023**, *35*, 2208517. https://doi.org/10.1002/adma.202208517.
16. Yeh, J.-W.; Chen, S.-K.; Lin, S.-J.; et al. Nanostructured High-Entropy Alloys with Multiple Principal Elements: Novel Alloy Design Concepts and Outcomes. *Adv. Eng. Mater.* **2004**, *6*, 299–303. https://doi.org/10.1002/adem.200300567.
17. Zhang, Y. Science and technology in high-entropy alloys. *Sci. China Mater.* **2018**, *61*, 2–22.
18. Pradeep, K.G.; Tasan, C.C.; Yao, M.J.; et al. Non-equiatomic high entropy alloys: Approach towards rapid alloy screening and property-oriented design. *Mater. Sci. Eng. A* **2015**, *648*, 183–192.
19. Miracle, D.B.; Senkov, O.N. A critical review of high entropy alloys and related concepts. *Acta Mater.* **2017**, *122*, 448–511. https://doi.org/10.1016/j.actamat.2016.08.081.
20. Song, X.; Liu, Z.; Liaw, P.K.; et al. Microstructures and precipitation behaviors of a hypoeutectic high-entropy alloy prepared by laser powder bed fusion. *Addit. Manuf.* **2024**, *85*, 104171.
21. Zhang, W.-T.; Wang, X.-Q.; Zhang, F.-Q.; et al. Frontiers in high entropy alloys and high entropy functional materials. *Rare Met.* **2024**, *43*, 4639–4776. https://doi.org/10.1007/s12598-024-02852-0.
22. Chang, J.; Wang, G.; Li, C.; et al. Rational design of septenary high-entropy alloy for direct ethanol fuel cells. *Joule* **2023**, *7*, 587–602. https://doi.org/10.1016/j.joule.2023.02.011.
23. Wu, Y.; Yue, Y.; Yan, X.; et al. Mechanical and corrosion behavior of $CoCrFeNiAl_{0.3}$ high entropy alloy seamless tubes. *J. Alloys Compd.* **2025**, *1010*, 177143. https://doi.org/10.1016/j.jallcom.2024.177143.
24. Bingnan, Q.; Xiaoqing, L.; Wei, Y.; et al. An Ultra-Low Modulus of Ductile TiZrHfTa Biomedical High-Entropy Alloys through Deformation Induced Martensitic Transformation/Twinning/Amorphization. *Adv. Mater.* **2024**, *36*, 202310926. https://doi.org/10.1002/adma.202310926.
25. Xu, L.; Du, H.; Liu, J.; et al. Microstructure, Mechanical, and Electrochemical Properties of SiC Particle Reinforced CoCrFeNiCu High-Entropy Alloy Coatings. *Coatings* **2022**, *12*, 519.
26. Gao, J.; Wang, X.; Zhang, S.; et al. Producing of FeCoNiCrAl high-entropy alloy reinforced Al composites via friction stir processing technology. *Int. J. Adv. Manuf. Technol.* **2020**, *110*, 569–580. https://doi.org/10.1007/s00170-020-05912-8.
27. Rao, Z.; Tung, P.Y.; Xie, R.; et al. Machine learning–enabled high-entropy alloy discovery. *Science* **2022**, *378*, 78–85. https://doi.org/10.1126/science.abo4940.
28. Chen, C.; Han, X.; Zhang, Y.; et al. Phase prediction of high-entropy alloys based on machine learning and an improved

information fusion approach. *Comput. Mater. Sci.* **2024**, *239*, 112976. https://doi.org/10.1016/j.commatsci.2024.112976.
29. Rickman, J.M.; Chan, H.M.; Harmer, M.P.; et al. Materials informatics for the screening of multi-principal elements and high-entropy alloys. *Nat. Commun.* **2019**, *10*, 2618. https://doi.org/10.1038/s41467-019-10533-1.
30. Huang, W.; Martin, P.; Zhuang, H.L. Machine-learning phase prediction of high-entropy alloys. *Acta Mater.* **2019**, *169*, 225–236. https://doi.org/10.1016/j.actamat.2019.03.012.
31. Farber, E.; Zhu, J.-N.; Popovich, A.A.; et al. A review of NiTi shape memory alloy as a smart material produced by additive manufacturing. *Mater. Today Proc.* **2020**, *30*, 761–767.
32. Sater, J.M.; Lab, A.F.W. Smart structures and materials 1997. In Proceedings of the Industrial and Commercial Applications of Smart Structures Technologies, San Diego, CA, USA, 4–6 March 1997.
33. Ölander, A. An electrochemical investigation of solid cadmium-gold alloys. *J. Am. Chem. Soc.* **1932**, *54*, 3819–3833. https://doi.org/10.1021/ja01349a004.
34. Buehler, W.J.; Gilfrich, J.V.; Wiley, R.C. Effect of Low-Temperature Phase Changes on the Mechanical Properties of Alloys near Composition TiNi. *J. Appl. Phys.* **1963**, *34*, 1475–1477. https://doi.org/10.1063/1.1729603.
35. Kauffman, G.B.; Mayo, I. The Story of Nitinol: The Serendipitous Discovery of the Memory Metal and Its Applications. *Chem. Educ.* **1997**, *2*, 1–21. https://doi.org/10.1007/s00897970111a.
36. Ullakko, K. Magnetically controlled shape memory alloys: A new class of actuator materials. *J. Mater. Eng. Perform.* **1996**, *5*, 405–409. https://doi.org/10.1007/BF02649344.
37. Chen, C.-H.; Chen, Y.-J. Shape memory characteristics of $(TiZrHf)_{50}Ni_{25}Co_{10}Cu_{15}$ high entropy shape memory alloy. *Scr. Mater.* **2019**, *162*, 185–189. https://doi.org/10.1016/j.scriptamat.2018.11.023.
38. Liu, D.; Zhu, J.; Ding, Z.; et al. Magnetic-field-induced twist in Ni-Mn-Ga-Co-Cu microwires. *Scr. Mater.* **2017**, *128*, 91–94. https://doi.org/10.1016/j.scriptamat.2016.09.041.
39. Pérez-Checa, A.; José María, P.; Feuchtwanger, J.; et al. Role of Fe addition in Ni–Mn–Ga–Co–Cu–Fe ferromagnetic shape memory alloys for high-temperature magnetic actuation. *Acta Mater.* **2020**, *196*, 549–555. https://doi.org/10.1016/j.actamat.2020.07.007.
40. Pérez-Checa, A.; Denys, M.; Andrey, S.; et al. Study of the critical parameters for magnetic field-induced strain in high temperature Ni-Mn-Ga-Co-Cu-Fe single crystals. *Scr. Mater.* **2019**, *158*, 16–19. https://doi.org/10.1016/j.scriptamat.2018.08.018.
41. Zider, R.B.; Krumme, J.F. Eyeglass Frame Including Shape-Memory Elements. U.S. Patent 4,896,955, 30 January 1990.
42. Hautcoeur, A.; Eberhardt, A. Eyeglass Frame with Very High Recoverable Deformability. U.S. Patent 5,640,217, 17 June 1997.
43. Degeratu, S.; Rotaru, P.; Boncea, I.; et al. An Overview of the Properties and Industrial Applications of Shape Memory Alloys. In Proceedings of the 2018 International Symposium on Fundamentals of Electrical Engineering (ISFEE), Bucharest, Romania, 1–3 November 2018. https://doi.org/10.1109/isfee.2018.8742410.
44. Yang, H.; Xu, M.; Li, W.; et al. Design and Implementation of a Soft Robotic Arm Driven by SMA Coils. *IEEE Trans. Ind. Electron.* **2018**, *66*, 6108–6116. https://doi.org/10.1109/tie.2018.2872005.
45. Tsimbo Fokou, M.R.; Xia, Q.; Jin, H.; et al. A Soft Robotic Fish Actuated by Artificial Muscle Modules (SoRoFAAM-1). *J. Bionic Eng.* **2023**, *20*, 2030–2043. https://doi.org/10.1007/s42235-023-00390-6.
46. Kumar, P.; Singh, J.; Kaur, D. Ferromagnetic Shape Memory Alloy Integrated Highly Flexible SAW Delay Line Magnetic Sensor. *IEEE Sens. J.* **2024**, *24*, 2664–2670. https://doi.org/10.1109/jsen.2023.3345031.
47. Pang, J.; Tian, J.; Dang, P.; et al. Attainment of large thermal hysteresis and good thermal cyclic stability in multi-component TiHfZrNi alloys. *Scr. Mater.* **2024**, *249*, 116164. https://doi.org/10.1016/j.scriptamat.2024.116164.
48. Li, H.F.; Fei, N.; Yufeng, Z.; et al. Nanocrystalline $Ti_{49.2}Ni_{50.8}$ shape memory alloy as orthopaedic implant material with better performance. *J. Mater. Sci. Technol.* **2019**, *35*, 2156–2162. https://doi.org/10.1016/j.jmst.2019.04.026.
49. Baitab, D.M.; Majid, D.L.A.H.A.; Abdullah, E.; et al. A review of techniques for embedding shape memory alloy (SMA) wires in smart woven composites. *Int. J. Eng. Technol.* **2018**, *7*, 129–136. https://doi.org/10.14419/ijet.v7i4.13.21344.
50. Gall, K.; Maier, H.J. Cyclic deformation mechanisms in precipitated NiTi shape memory alloys. *Acta Mater.* **2002**, *50*, 4643–4657. https://doi.org/10.1016/s1359-6454(02)00315-4.
51. Morin, C.; Moumni, Z.; Zaki, W. Thermomechanical coupling in shape memory alloys under cyclic loadings: Experimental analysis and constitutive modeling. *Int. J. Plast.* **2011**, *27*, 1959–1980. https://doi.org/10.1016/j.ijplas.2011.05.005.
52. Wei, P.; Hua, P.; Xia, M.; et al. Bending fatigue life enhancement of NiTi alloy by pre-strain warm surface mechanical attrition treatment. *Acta Mater.* **2022**, *240*, 118269. https://doi.org/10.1016/j.actamat.2022.118269.
53. Benafan, O.; Brown, J.; Calkins, F.T.; et al. Shape memory alloy actuator design: CASMART collaborative best practices and case studies. *Int. J. Mech. Mater. Des.* **2014**, *10*, 1–42. https://doi.org/10.1007/s10999-013-9227-9.
54. Lagoudas, D.C.; Entchev, P.B.; Popov, P.; et al. Shape memory alloys, Part II: Modeling of polycrystals. *Mech. Mater.* **2006**, *38*, 430–462. https://doi.org/10.1016/j.mechmat.2005.08.003.

55. Wang, W.; Ji, Y.; Fang, M.; et al. Reentrant strain glass transition in Ti-Ni-Cu shape memory alloy. *Acta Mater.* **2022**, *226*, 117618. https://doi.org/10.1016/j.actamat.2022.117618.
56. Zhu, J.N.; Zhu, W.; Borisov, E.; et al. Effect of heat treatment on microstructure and functional properties of additively manufactured NiTi shape memory alloys. *J. Alloys Compd.* **2023**, *967*, 171740. https://doi.org/10.1016/j.jallcom.2023.171740.
57. Jena, D.; Dora, T.R.K.; Vardhan, A.V.; et al. Micro-texture and residual stress evolution in shot peened superelastic Ni-Ti/Ni-Ti-Co shape memory alloys. *Surf. Coat. Technol.* **2024**, *479*, 130529. https://doi.org/10.1016/j.surfcoat.2024.130529.
58. Milyutin, V.A.; Bureš, R.; Fáberová, M.; et al. Multi-component soft magnetic alloy $FeNiCoAl_{0.4}Mo_{0.1}Si_{0.4}B_{0.1}$ with high frequency stability of permeability. *Mater. Sci. Eng. B* **2023**, *293*, 116485. https://doi.org/10.1016/j.mseb.2023.116485.
59. Cai, M.; Wang, J.; Wang, Q.; et al. Improvement of soft-magnetic properties for Fe-based amorphous alloys with high saturation polarization by stress annealing. *Mater. Res. Lett.* **2023**, *11*, 595–603. https://doi.org/10.1080/21663831.2023.2199044.
60. Li, X.; Zhou, J.; Shen, L.; et al. Exceptionally High Saturation Magnetic Flux Density and Ultralow Coercivity via an Amorphous–Nanocrystalline Transitional Microstructure in an FeCo-Based Alloy. *Adv. Mater.* **2022**, *35*, 2205863. https://doi.org/10.1002/adma.202205863.
61. Premkumar, M.; Mitra, A.; Arun, P.; et al. Magnetostriction of Fe-rich FeSiB(P)NbCu amorphous and nanocrystalline soft-magnetic alloys. *J. Alloys Compd.* **2023**, *960*, 170760. https://doi.org/10.1016/j.jallcom.2023.170760.
62. Luo, T.; Xu, J.; Wang, G.; et al. Composition dependence of amorphous forming, crystallization behavior, magnetic and electronic properties of silicon-rich FeSiBCuNb alloys. *J. Magn. Magn. Mater.* **2020**, *505*, 166714. https://doi.org/10.1016/j.jmmm.2020.166714.
63. Haneczok, G.; Wroczyński, R.; Kwapuliński, P.; et al. Electro/magnetic shielding effectiveness of soft magnetic Fe80Nb6B14 amorphous alloy. *J. Mater. Process. Technol.* **2009**, *209*, 2356–2360. https://doi.org/10.1016/j.jmatprotec.2008.05.026.
64. Zhou, J.; Li, X.; Hou, X.; et al. Ultrahigh Permeability at High Frequencies via A Magnetic-Heterogeneous Nanocrystallization Mechanism in an Iron-Based Amorphous Alloy. *Adv. Mater.* **2023**, *35*, 2304490. https://doi.org/10.1002/adma.202304490.
65. Chen, Z.; Kang, S.; Zhu, Q.; et al. Tailoring the thermal stability and soft magnetic properties of Fe_{80}-Ni $Si_7B_8P_4Cu_1$ amorphous nanocrystalline alloys based on the magnetic domain structure. *J. Alloys Compd.* **2023**, *968*, 172116. https://doi.org/10.1016/j.jallcom.2023.172116.
66. Zanaeva, E.N.; Bazlov, A.I.; Milkova, D.A.; et al. High-Frequency soft magnetic properties of Fe-Si-B-P-Mo-Cu amorphous and nanocrystalline alloys. *J. Non-Cryst. Solids* **2019**, *526*, 9702. https://doi.org/10.1016/j.jnoncrysol.2019.119702.
67. Li, J.; Yu, H.; Luo, P.; et al. Effects of Phosphating Treatment on the Growth of a Phosphate Layer and the Magnetic Properties of Fe-Based Amorphous Magnetic Powder Cores. *J. Electron. Mater.* **2023**, *52*, 5412–5421. https://doi.org/10.1007/s11664-023-10437-3.
68. Tokmakova, E.N.; Vvedenskiy, V.Y. Effect of annealing in unsaturated magnetic field on the magnetic properties of an amorphous alloy Fe77Ni1Si9B13. *J. Mater. Sci. Mater. Electron.* **2023**, *34*, 1509. https://doi.org/10.1007/s10854-023-10931-8.
69. Lin, J.; Li, X.; Zhou, S.; et al. Effects of heat treatment in air on soft magnetic properties of FeCoSiBPC amorphous core. *J. Non-Cryst. Solids* **2022**, *597*, 121932. https://doi.org/10.1016/j.jnoncrysol.2022.121932.
70. Luo, T.; Yang, Y.; Fan, C.; et al. Effects of phosphorus substitution on amorphous formation, crystallization behavior and magnetic properties of FeSiBCuNb alloys. *J. Non-Cryst. Solids* **2022**, *576*, 1286. https://doi.org/10.1016/j.jnoncrysol.2021.121286.
71. Li, Y.L.; Dou, Z.X.; Chen, X.M.; et al. Improving the amorphous forming ability and magnetic properties of FeSiBPCu amorphous and nanocrystalline alloys by utilizing carbon. *J. Alloys Compd.* **2020**, *844*, 155767. https://doi.org/10.1016/j.jallcom.2020.155767.
72. Li, W.; Yang, Y.H.; Xie, C.X.; et al. Glass formation, crystallization and magnetic properties of high-Fe Fe-metalloid (B, C, and P) melt-spun ribbons. *J. Magn. Magn. Mater.* **2020**, *498*, 166128. https://doi.org/10.1016/j.jmmm.2019.166128.
73. Pang, L.L.; Inoue, A.; Zanaeva, E.N.; et al. Nanocrystallization, good soft magnetic properties and ultrahigh mechanical strength for $Fe_{82\text{-}85}B_{13\text{-}16}Si_1Cu_1$ amorphous alloys. *J. Alloys Compd.* **2019**, *785*, 25–37. https://doi.org/10.1016/j.jallcom.2019.01.150.
74. Lu, S.; Wang, M.; Zhao, Z. Recent advances and future developments in Fe-based amorphous soft magnetic composites. *J. Non-Cryst. Solids* **2023**, *616*, 122440. https://doi.org/10.1016/j.jnoncrysol.2023.122440.
75. Chaudhary, V.; Chaudhary, R.; Banerjee, R.; et al. Accelerated and conventional development of magnetic high entropy alloys. *Mater. Today* **2021**, *49*, 231–252. https://doi.org/10.1016/j.mattod.2021.03.018.

76. Liu, M.; Lei, C.; Wang, Y.; et al. High-throughput preparation for alloy composition design in additive manufacturing: A comprehensive review. *Mater. Genome Eng. Adv.* **2024**, *2*, e55. https://doi.org/10.1002/mgea.55.
77. Li, Z.; Ludwig, A.; Savan, A.; et al. Combinatorial metallurgical synthesis and processing of high-entropy alloys. *J. Mater. Res.* **2018**, *33*, 3156–3169. https://doi.org/10.1557/jmr.2018.214.
78. Li, W.; Xie, D.; Li, D.; et al. Mechanical behavior of high-entropy alloys. *Prog. Mater. Sci.* **2021**, *118*, 100777. https://doi.org/10.1016/j.pmatsci.2021.100777.
79. Borkar, T.; Gwalani, B.; Choudhuri, D.; et al. A combinatorial assessment of AlxCrCuFeNi2 ($0 < x < 1.5$) complex concentrated alloys: Microstructure, microhardness, and magnetic properties. *Acta Mater.* **2016**, *116*, 63–76. https://doi.org/10.1016/j.actamat.2016.06.025.
80. Moorehead, M.; Bertsch, K.; Niezgoda, M.; et al. High-throughput synthesis of Mo-Nb-Ta-W high-entropy alloys via additive manufacturing. *Mater. Des.* **2020**, *187*, 108358. https://doi.org/10.1016/j.matdes.2019.108358.
81. Akbari, A.; Balk, T.J. Combinatorial thin film screening to identify single-phase, non-equiatomic high entropy alloys in the MnFeCoNiCu system. *MRS Commun.* **2019**, *9*, 750–755. https://doi.org/10.1557/mrc.2019.53.
82. Shang, G.; Jiang, L.; Liu, Z.Z.; et al. High-throughput experimental study on the microstructural and compositional variations of mechanical properties for AlCoCrFeNi high entropy alloys. *J. Alloys Compd.* **2022**, *917*, 165513. https://doi.org/10.1016/j.jallcom.2022.165513.
83. Zhao, L.; Zhou, Y.; Wang, H.; et al. High-Throughput Synthesis and Characterization of a Combinatorial Materials Library in Bulk Alloys. *Metall. Mater. Trans.* **2021**, *52*, 1159–1168. https://doi.org/10.1007/s11661-021-06149-0.
84. Wang, C.; Han, K.; Liu, X.; et al. First-principles study of hydrogen-vacancy interactions in CoCrFeMnNi high-entropy alloy. *J. Alloys Compd.* **2022**, *922*, 166259. https://doi.org/10.1016/j.jallcom.2022.166259.
85. Yu, P.; Feng, R.; Du, J.; et al. Phase transformation assisted twinning in a face-centered-cubic FeCrNiCoAl high entropy alloy. *Acta Mater.* **2019**, *181*, 491–500. https://doi.org/10.1016/j.actamat.2019.10.012.
86. Zhang, Z.Q.; Ketov, S.V.; Fellner, S.; et al. Reactive interdiffusion of an Al film and a CoCrFeNi high-entropy alloy. *Mater. Des.* **2022**, *216*, 110530. https://doi.org/10.1016/j.matdes.2022.110530.
87. Yin, B.; Yoshida, S.; Tsuji, N.; et al. Yield strength and misfit volumes of NiCoCr and implications for short-range-order. *Nat. Commun.* **2020**, *11*, 2507. https://doi.org/10.1038/s41467-020-16083-1.
88. Wu, M.; Wang, S.; Huang, H.; et al. CALPHAD aided eutectic high-entropy alloy design. *Mater. Lett.* **2020**, *262*, 127175. https://doi.org/10.1016/j.matlet.2019.127175.
89. Zhao, D.; Jin, X.; Qiao, J.; et al. Machine-learning-assisted modeling of alloy ordering phenomena at the electronic scale through electronegativity. *Appl. Phys. Lett.* **2024**, *124*, 0188516. https://doi.org/10.1063/5.0188516.
90. Guo, C.; Wei, S.; Wu, Z.; et al. Effect of dual phase structure induced by chemical segregation on hot tearing reduction in additive manufacturing. *Mater. Des.* **2023**, *228*, 111847. https://doi.org/10.1016/j.matdes.2023.111847.
91. Men, Y.; Wu, D.; Hu, Y.; et al. Understanding Alkaline Hydrogen Oxidation Reaction on PdNiRuIrRh High-Entropy-Alloy by Machine Learning Potential. *Angew. Chem. Int. Ed.* **2023**, *62*, e202217976. https://doi.org/10.1002/anie.202217976.
92. Ren, J.C.; Zhou, J.; Butch, C.J.; et al. Predicting single-phase solid solutions in as-sputtered high entropy alloys: High-throughput screening with machine-learning model. *J. Mater. Sci. Technol.* **2023**, *138*, 70–79. https://doi.org/10.1016/j.jmst.2022.07.059.
93. Singh, S.; Katiyar, N.K.; Goel, S.; et al. Phase prediction and experimental realisation of a new high entropy alloy using machine learning. *Sci. Rep.* **2023**, *13*, 4811. https://doi.org/10.1038/s41598-023-31461-7.
94. He, S.; Wang, Y.; Zhang, Z.; et al. Interpretable machine learning workflow for evaluation of the transformation temperatures of TiZrHfNiCoCu high entropy shape memory alloys. *Mater. Des.* **2023**, *225*, 111513. https://doi.org/10.1016/j.matdes.2022.111513.
95. Kumar, S.; Pradhan, H.; Shah, N.; et al. Machine learning enabled processing map generation for high-entropy alloy. *Scr. Mater.* **2023**, *234*, 115543. https://doi.org/10.1016/j.scriptamat.2023.115543.
96. Kumar, N.; Sarkar, S.; Anand, T.N.C.; et al. Estimating metal mass flowrate in gas-atomization for metal powder production. *Powder Technol.* **2024**, *448*, 120238. https://doi.org/10.1016/j.powtec.2024.120238.
97. Steven, P.M.; Gary, S.S. A study of liquid metal atomization using close-coupled nozzles, part 1: Gas dynamic behavior. *At. Sprays* **2005**, *15*, 19–40. https://doi.org/10.1615/atomizspr.v15.i1.20.
98. Alvarez, K.L.; Baghbaderani, H.A.; Martín, J.M.; et al. Novel Fe-based amorphous and nanocrystalline powder cores for high-frequency power conversion. *J. Magn. Magn. Mater.* **2020**, *501*, 166457. https://doi.org/10.1016/j.jmmm.2020.166457.
99. Chang, J.; Zhan, T.; Peng, X.; et al. Improved permeability and core loss of amorphous FeSiB /Ni-Zn ferrite soft magnetic composites prepared in an external magnetic field. *J. Alloys Compd.* **2021**, *886*, 161335. https://doi.org/10.1016/j.jallcom.2021.161335.
100. Wang, P.; Zhu, Z.; Liu, J.; et al. Soft magnetic properties regulation of FeSiBC amorphous powders/CIP magnetic powder

core with single and double-layer core–shell structure. *J. Magn. Magn. Mater.* **2023**, *578*, 170809. https://doi.org/10.1016/j.jmmm.2023.170809.

101. Conteri, R.; Borkar, T.; Nag, S.; et al. Laser additive processing of Fe-Si-B-Cu-Nb magnetic alloys. *J. Manuf. Process.* **2017**, *29*, 175–181. https://doi.org/10.1016/j.jmapro.2017.07.029.
102. Zhao, Y.; Bai, Y.; Li, T.; et al. Microstructure and Superelasticity of Cu–Sn Shape-Memory Microwires by Glass-Coated Melt Spinning. *Metals* **2023**, *13*, 1852. https://doi.org/10.3390/met13111852.
103. Salaheldeen, M.; Garcia-Gomez, A.; Corte-León, P.; et al. Manipulation of magnetic and structure properties of Ni2FeSi glass-coated microwires by annealing. *J. Alloys Compd.* **2023**, *942*, 169026. https://doi.org/10.1016/j.jallcom.2023.169026.
104. Komova, E.; Varga, M.; Varga, R.; et al. Nanocrystalline glass-coated FeNiMoB microwires. *Appl. Phys. Lett.* **2008**, *93*, 062502. https://doi.org/10.1063/1.2969057.
105. Khatun, H.; Nath, S.D.; Sikder, S.S. Kinetics of crystallization and soft magnetic properties of $Co_{72}Fe_8B_{10}Si_{10}$ amorphous alloys. *Phys. B Condens.* **2024**, *691*, 416300.
106. Amini, N.; Miglierini, M.; Hasiak, M.; et al. Thickness Dependence of Mössbauer Parameters for $Fe_{78}Si_9B_{13}$ Metallic Glass Ribbons. *Acta Phys. Pol. A* **2017**, *131*, 666–668. https://doi.org/10.12693/aphyspola.131.666.
107. Ma, Y.; Kou, Z.; Yang, W.; et al. A one-step fabrication of soft-magnetic high entropy alloy fiber with excellent strength and flexibility. *Nat. Commun.* **2024**, *15*, 10549. https://doi.org/10.1038/s41467-024-54984-7.
108. Xu, Z.; Ji, Y.; Liu, C.; et al. A polymer-like ultrahigh-strength metal alloy. *Nature* **2024**, *633*, 575–581. https://doi.org/10.1038/s41586-024-07900-4.
109. Liu, G.; Li, S.; Song, C.; et al. High-entropy Ti-Zr-Hf-Ni-Cu alloys as solid-solid phase change materials for high-temperature thermal energy storage. *Intermetallics* **2024**, *166*, 108177. https://doi.org/10.1016/j.intermet.2023.108177.
110. Li, H.X.; Lu, Z.C.; Wang, S.L.; et al. Fe-based bulk metallic glasses: Glass formation, fabrication, properties and applications. *Prog. Mater. Sci.* **2019**, *103*, 235–318. https://doi.org/10.1016/j.pmatsci.2019.01.003.
111. He, S.; Zhou, X.; Mordehai, D.; et al. Thermal super-jogs control the high-temperature strength plateau in Nb-Mo-Ta-W alloys. *Acta Mater.* **2023**, *244*, 118539. https://doi.org/10.1016/j.actamat.2022.118539.
112. Hua, P.; Xia, M.; Onuki, Y.; et al. Nanocomposite NiTi shape memory alloy with high strength and fatigue resistance. *Nat. Nanotechnol.* **2021**, *16*, 409–413. https://doi.org/10.1038/s41565-020-00837-5.
113. Eggert, B.G.; Delczeg-Czirjak, E.K.; Maccari, F.; et al. Exploring V-Fe-Co-Ni-Al and V-Fe-Co-Ni-Cu high entropy alloys for magnetocaloric applications. *J. Alloys Compd.* **2022**, *921*, 166040. https://doi.org/10.1016/j.jallcom.2022.166040.
114. Nai, X.; Chen, H.; Zhao, S.; et al. Investigation on the microstructure, mechanical and electrical properties of Ti_3SiC_2/Cu joint obtained by $Ti_{25}Zr_{25}Ni_{25}Cu_{25}$ amorphous high entropy alloy and Ag composite filler. *Mater. Sci. Eng. A* **2023**, *877*, 145190. https://doi.org/10.1016/j.msea.2023.145190.